Downloaded from http://rupress.org/jgp/article-pdf/144/2/181/1793677/jgp\_201411191.pdf by guest on 03 December 2025

# The conserved potassium channel filter can have distinct ion binding profiles: Structural analysis of rubidium, cesium, and barium binding in NaK2K

Yee Ling Lam, 1 Weizhong Zeng, 1,2 David Bryant Sauer, 1 and Youxing Jiang 1,2

<sup>1</sup>Department of Physiology and <sup>2</sup>Howard Hughes Medical Institute, University of Texas Southwestern Medical Center, Dallas, TX 75390

Potassium channels are highly selective for  $K^+$  over the smaller  $Na^+$ . Intriguingly, they are permeable to larger monovalent cations such as  $Rb^+$  and  $Cs^+$  but are specifically blocked by the similarly sized  $Ba^{2+}$ . In this study, we used structural analysis to determine the binding profiles for these permeant and blocking ions in the selectivity filter of the potassium-selective NaK channel mutant NaK2K and also performed permeation experiments using single-channel recordings. Our data revealed that some ion binding properties of NaK2K are distinct from those of the canonical  $K^+$  channels KcsA and MthK.  $Rb^+$  bound at sites 1, 3, and 4 in NaK2K, as it does in KcsA.  $Cs^+$ , however, bound predominantly at sites 1 and 3 in NaK2K, whereas it binds at sites 1, 3, and 4 in KcsA. Moreover,  $Ba^{2+}$  binding in NaK2K was distinct from that which has been observed in KcsA and MthK, even though all of these channels show similar  $Ba^{2+}$  block. In the presence of  $K^+$ ,  $Ba^{2+}$  bound to the NaK2K channel at site 3 in conjunction with a  $K^+$  at site 1; this led to a prolonged block of the channel (the external  $K^+$ -dependent  $Ba^{2+}$  lock-in state). In the absence of  $K^+$ , however,  $Ba^{2+}$  acts as a permeating blocker. We found that, under these conditions,  $Ba^{2+}$  bound at sites 1 or 0 as well as site 3, allowing it to enter the filter from the intracellular side and exit from the extracellular side. The difference in the  $Ba^{2+}$  binding profile in the presence and absence of  $K^+$  thus provides a structural explanation for the short and prolonged  $Ba^{2+}$  block observed in NaK2K.

#### INTRODUCTION

The Journal of General Physiology

Rapid and selective conduction of potassium ions across cell membranes is central to many biological processes, including nerve excitation, muscle cell contraction, signal transduction, and hormone secretion (Hille, 2001). These are two seemingly mutually exclusive properties, as high selectivity is normally achieved by high affinity ion binding, whereas the opposite is required for a high flux rate. With an ingenious architecture in the channel pore, tetrameric potassium channels can specifically allow K<sup>+</sup> ions to permeate and traverse down their electrochemical gradients at a rate close to the diffusion limit. The pore of K<sup>+</sup> channels has a unique structure known as the selectivity filter, which is formed by the conserved signature sequence TVGYGD (Heginbotham et al., 1994). Within the selectivity filter, the backbone carbonyl oxygen atoms from the TVGY residues and the hydroxyl oxygen from the threonine side chain point toward the center and form four contiguous ion-binding sites (numbered 1-4 from the extracellular side) for dehydrated K<sup>+</sup> ions (Fig. 1), mimicking the hydration

As Na<sup>+</sup> and K<sup>+</sup> are the two most abundant cations in life, K<sup>+</sup> channels appear to have evolved to achieve high selectivity primarily by the exclusion of smaller sodium ions. Indeed, K<sup>+</sup> channels select poorly among ions that are of a similar size as or slightly larger than K<sup>+</sup>, such as Rb<sup>+</sup>, Cs<sup>+</sup>, and Tl<sup>+</sup>. Some K<sup>+</sup> channels are actually more selective for Rb<sup>+</sup> or Cs<sup>+</sup> than K<sup>+</sup> (Eisenman et al., 1986; Heginbotham and MacKinnon, 1993; LeMasurier et al., 2001). However, the conduction of these larger ions in the K<sup>+</sup> channel is not as efficient as that of K<sup>+</sup>, likely because of the imbalanced ion distribution in the filter. The Ba<sup>2+</sup> ion, which has the same size as K<sup>+</sup> but twice the

shell of a K<sup>+</sup> ion (Doyle et al., 1998; Zhou et al., 2001). Having four contiguous ion-binding sites in the filter has been shown to be a prerequisite for selective K<sup>+</sup> conduction, and structural deviation from the four-site filter architecture will lead to the loss of selectivity (Derebe et al., 2011a; Sauer et al., 2011). During permeation, two K<sup>+</sup> ions occupy the four-site filter with equal probability, most likely hopping between 1,3 and 2,4 configurations. This equal distribution of two conducting ions within the filter is necessary for efficient ion permeation (Morais-Cabral et al., 2001).

Y.L. Lam, W. Zeng, and D.B. Sauer contributed equally to this paper. Correspondence to Youxing Jiang: youxing.jiang@utsouthwestern.edu

D.B. Sauer's present address is The Helen L. and Martin S. Kimmel Center for Biology and Medicine, Skirball Institute of Biomolecular Medicine, New York University School of Medicine, New York, NY 10016.

Abbreviations used in this paper: DM, n-decyl- $\beta$ -D-maltoside; MPD,  $(\pm)$ -2-methyl-2,4-pentanediol; RMSD, root mean square deviation.

<sup>© 2014</sup> Lam et al. This article is distributed under the terms of an Attribution–Noncommercial–Share Alike–No Mirror Sites license for the first six months after the publication date (see http://www.rupress.org/terms). After six months it is available under a Creative Commons License (Attribution–Noncommercial–Share Alike 3.0 Unported license, as described at http://creativecommons.org/licenses/by-nc-sa/3.0/).

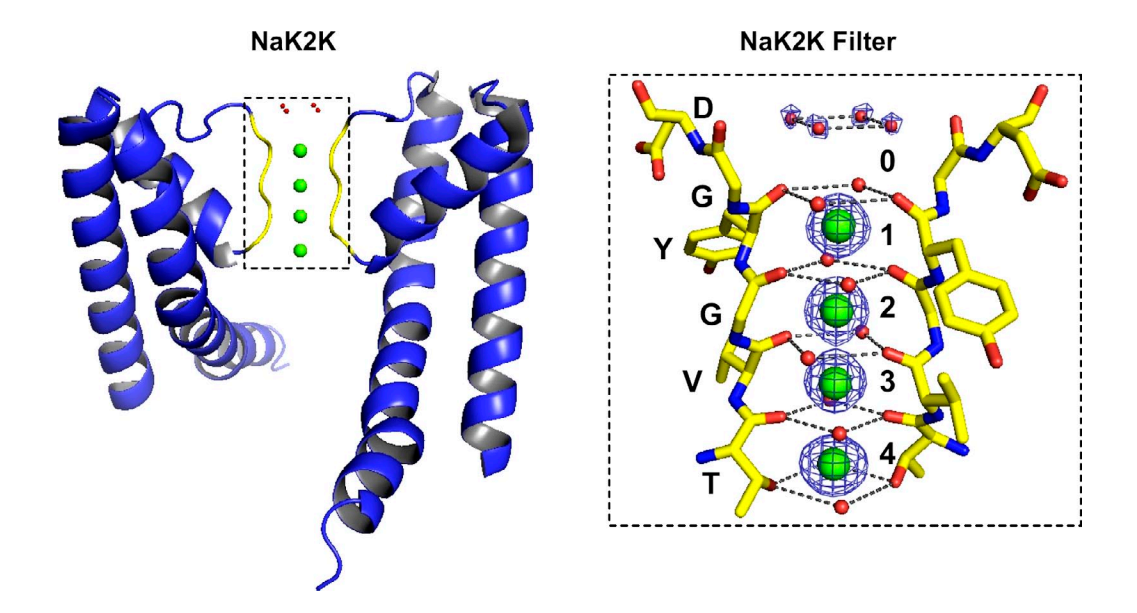


Figure 1. Overall structure of the NaK2K-K $^+$  complex in open conformation with the front and back subunits removed for clarity. A magnified view of its selectivity filter (boxed) is shown. Electron density (blue mesh) from the  $F_o$ - $F_c$  ion omit map (4 $\sigma$ ) shows  $K^+$  ions (modeled as green spheres) in the filter and water molecules (modeled as red spheres) at site 0. The four ion-binding sites within the filter are labeled 1–4 from top to bottom.

charge, binds to the K<sup>+</sup> channel filter with higher affinity and blocks the K<sup>+</sup> flux. This blocking property of Ba<sup>2+</sup> has been studied extensively to probe the selectivity and multi-ion features of K<sup>+</sup> channels long before the determination of the first K<sup>+</sup> channel structure (Armstrong and Taylor, 1980; Eaton and Brodwick, 1980; Armstrong et al., 1982; Vergara and Latorre, 1983; Miller, 1987; Neyton and Miller, 1988a,b; Harris et al., 1998; Vergara et al., 1999; Piasta et al., 2011).

The ion-binding profile of these permeating and blocking ions for K<sup>+</sup> channels has been structurally defined in KcsA (Jiang and MacKinnon, 2000; Zhou and MacKinnon, 2003; Lockless et al., 2007), a prototypic K<sup>+</sup> channel that has been commonly used as a model system to study K<sup>+</sup> selectivity (Alam and Jiang, 2011; Andersen, 2011; Dixit and Asthagiri, 2011; Nimigean and Allen, 2011; Roux et al., 2011; Varma et al., 2011). Recently, our structural studies of the nonselective NaK channel and its mutants have provided us an alternative model system for precise examination of ion binding and selectivity of both K<sup>+</sup>-selective and nonselective channels. The use of NaK and its mutant channels has several advantages: all of these channels have high resolution structures; their crystals can be manipulated in various salt solutions without compromising the crystal diffraction quality; and the channels can be functionally characterized by single-channel recording using giant liposome patch (Derebe et al., 2011a,b; Sauer et al., 2011, 2013). In this study, we used the K<sup>+</sup>-selective NaK mutant NaK2K (Fig. 1) to examine the ion binding as well as permeation properties for Rb<sup>+</sup>, Cs<sup>+</sup>, and Ba<sup>2+</sup>. Our results demonstrate

that Cs<sup>+</sup> and Ba<sup>2+</sup> binding in NaK2K is different from that observed in KcsA, despite the fact that both channels have a virtually identical selectivity filter structure and similar ion permeation and blockage properties. In addition, Ba<sup>2+</sup> has a different binding profile within the NaK2K filter in the presence and absence of K<sup>+</sup>, and this K<sup>+</sup>-dependent difference in Ba<sup>2+</sup> occupancy provides structural insight into the Ba<sup>2+</sup> lock-in effect in K<sup>+</sup> channels.

#### MATERIALS AND METHODS

#### Protein expression, purification, and crystallization

K<sup>+</sup>-selective NaK double mutant NaK2K, containing the mutations D66Y and N68D, was encoded in the pQE-60 vector, expressed in the *Escherichia coli* strain SG13009, and purified as previously described (Derebe et al., 2011a). In brief, expression was induced with 0.4 mM IPTG (isopropyl-β-D-1-thiogalactopyranoside) in the presence of 5 mM BaCl<sub>2</sub> for 18 h at 25°C. Cells were lysed in 100 mM KCl and 50 mM Tris-HCl, pH 8.0, and the expressed channel proteins were solubilized with 40 mM *n*-decyl-β-D-maltoside (DM) and purified on a column (Talon IMAC; Takara Bio Inc.). Eluted proteins were digested overnight with thrombin, 1 U thrombin/2 mg protein, and further purified on a (10/30) size exclusion column (Superdex-200; GE Healthcare) in 100 mM KCl, 20 mM Tris-HCl, pH 8.0, and 4 mM DM. The NaK2K channel used in functional studies contains an additional mutation, F92A, which increases flux through the channel.

Purified NaK2K channels were concentrated to  $\sim \! 20~{\rm mg~ml}^{-1}$  and crystallized in the same conditions previous described using sitting drop vapor diffusion at 20°C (Alam and Jiang, 2009a). All crystals were initially grown in complex with K<sup>+</sup> by mixing equal volumes of protein solution (which contained 100 mM KCl) with a well solution of 62.5–70% (±)-2-methyl-2,4-pentanediol (MPD) and 100 mM buffer at various pH (Mes for pH 6.0–6.5, HEPES for pH 7.0–7.5). In all soaking experiments, the crystal was soaked

TABLE 1

Data collection and refinement statistics for NaK2K in complex with  $Rb^+$ ,  $Cs^+$ , or  $Ba^{2+}$ 

| Statistic                            | Protein               |                       |                                 |                                  |  |
|--------------------------------------|-----------------------|-----------------------|---------------------------------|----------------------------------|--|
|                                      | NaK2K-Rb <sup>+</sup> | NaK2K-Cs <sup>+</sup> | NaK2K–Ba <sup>2+</sup> (in KCl) | NaK2K-Ba <sup>2+</sup> (in NaCl) |  |
| Data collection                      |                       |                       |                                 |                                  |  |
| Space group                          | ${f I_4}$             | ${f I}_4$             | ${f I}_4$                       | ${ m I}_4$                       |  |
| Cell dimensions a = b, c (Å)         | 68.011, 89.346        | 68.106, 89.593        | 68.065, 89.614                  | 68.042, 89.627                   |  |
| Wavelength (Å)                       | 1.0000                | 1.0000                | 0.9999                          | 0.9793                           |  |
| Resolution (Å)                       | 50-1.58               | 50-1.70               | 50-1.82                         | 50-1.85                          |  |
| $R_{\text{sym}}$ (%)                 | 4.9 (78.6)            | 4.3 (77.0)            | 5.4 (99.8)                      | 6.3 (93.1)                       |  |
| /σΙ                                  | 48.3 (2.1)            | 49.8 (1.7)            | 37.0 (1.8)                      | 39.2 (2.3)                       |  |
| Number of total reflections (unique) | 205,718 (27,782)      | 165,736 (22,437)      | 128,478 (18,212)                | 130,140 (17,542)                 |  |
| Completeness (%)                     | 99.86 (99.82)         | 99.86 (99.64)         | 99.53 (100.00)                  | 99.24 (99.9)                     |  |
| Redundancy                           | 7.4 (7.3)             | 7.4 (6.8)             | 7.1 (7.2)                       | 7.4 (7.0)                        |  |
| Refinement                           |                       |                       |                                 |                                  |  |
| Resolution (Å)                       | 1.58                  | 1.70                  | 1.82                            | 1.85                             |  |
| $R_{ m work}/R_{ m free}$            | 0.2043/0.2335         | 0.2070/0.2358         | 0.1972/0.2324                   | 0.1998/0.2266                    |  |
| Number of atoms                      |                       |                       |                                 |                                  |  |
| Protein                              | 1,485                 | 1,485                 | 1,485                           | 1,485                            |  |
| MPD/ion                              | 3/6                   | 3/6                   | 4/9                             | 4/8                              |  |
| Vater                                | 79                    | 49                    | 63                              | 63                               |  |
| RMSD                                 |                       |                       |                                 |                                  |  |
| Bond angles (Å)                      | 0.007                 | 0.008                 | 0.008                           | 0.008                            |  |
| Bond lengths (Å)                     | 1.07                  | 1.08                  | 1.20                            | 1.09                             |  |

Values in parentheses are for the highest resolution shell. 5% of the data was used in the  $R_{\rm free}$  calculation.

overnight in stabilization solution containing 70% MPD, 10 mM DM, 100 mM Mes-NaOH, pH 6.0, and 100 mM XCl (X = Na, K, Rb, or Cs). For barium soaking, the stabilization solutions with 100 mM KCl or NaCl were supplemented with 20 mM BaCl $_2$ . All crystals were flash frozen in liquid nitrogen with the stabilization solution serving as cryoprotectant. All crystals were of the I4 space group, with unit cell dimensions around a = b = 68 Å, c = 89 Å, and contained two molecules (subunits A and B) in the asymmetric unit. The fourfold axis of channel tetramer coincided with the crystallographic tetrad. Only the tetramer generated from subunit A was used for structural analysis in this study, as the filter residues of this subunit have much lower and more stable B factors.

#### Data collection and structure determination

X-ray diffraction data were collected at the Advanced Light Source beamlines 8.2.1 and 8.2.2 and the Advanced Photon Source beamlines 19ID and 23ID. Data were processed and scaled in HKL-2000 (HKL Research, Inc.; Otwinowski and Minor, 1997). As all crystals for the soaking experiment were obtained from the same crystallization conditions as the previously determined NaK2K structure (Derebe et al., 2011a), the NaK2K-K+ complex structure (Protein Data Bank accession no. 3OUF) was directly used in the refinement against the diffraction data of each soaked crystal in Phenix (Adams et al., 2010) with solvent molecules and filter ions omitted. Before final refinement, the filter ions from soaking conditions and the solvent molecules were then placed with Coot (Emsley and Cowtan, 2004) using F<sub>o</sub>-F<sub>c</sub> ion omit maps. Data from all soaked crystals were scaled against the original NaK2K-K+ complex crystal before refinement and map calculation. Onedimensional electron density profiles through the filter were calculated as previously described (Morais-Cabral et al., 2001) by sampling the F<sub>o</sub>-F<sub>c</sub> ion omit maps (all calculated at 1.85 Å) along the C axis (which coincides with the molecular fourfold axis of channel tetramer) using MAPMAN (Kleywegt and Jones, 1996).

For occupancy estimation, the total area of the four peaks above the baseline in the one-dimensional electron density profile was set to represent electrons from two K<sup>+</sup> ions and two water molecules in the NaK2K–K<sup>+</sup> complex (total of 56 e-). The area of individual peak in the one-dimensional profile of various soaked crystals was then normalized against the peaks of the NaK2K–K<sup>+</sup> complex to calculate the number of electrons each peak represents; ion occupancy at each site was then calculated using the following equation, assuming a total occupancy of 1 for water (10 e-) and ion (N e-) at each site.  $N \times Y + 10 \times (1 - Y) = \text{number of electrons}$  calculated from the peak area (1), where N is the number of electrons for each filter ion (18 for K<sup>+</sup>, 36 for Rb<sup>+</sup>, and 54 for Cs<sup>+</sup> and Ba<sup>2+</sup>) and Y is the occupancy for the respective ion.

## Electrophysiology

All single-channel recordings were performed using giant liposome patches as described previously (Derebe et al., 2011a,b). A protein/lipid (3:1 POPE/POPG) ratio of 0.05–0.1 μg/mg was used to reconstitute proteoliposomes. Giant liposomes were obtained by air drying 2-3 µl liposome sample on a clean coverslip overnight at 4°C followed by rehydration in bath solution at room temperature. Patch pipettes were pulled from borosilicate glass (Harvard Apparatus) to a resistance of 8–12 M $\Omega$  filled with pipette solution containing 150 mM XCl, 1 mM EGTA, and 10 mM HEPES, pH 7.4, buffered with NaOH, where X is the monovalent cation (or mixed cations) used in each experiment, as discussed in the Results section, with a total concentration of 150 mM. The initial bath solution contained 150 mM KCl, 10 mM HEPES, and 1 mM EGTA, pH 7.4, buffered with Tris. A gigaseal (>10 G $\Omega$ ) was obtained by gentle suction when the patch pipette attached to the giant liposome. To get a single layer of membrane in the patch, the pipette was pulled away from the giant liposome, and the tip was exposed to air for 1-2 s. Membrane voltage was controlled and current recorded using an amplifier (Axopatch 200B; Molecular Devices)

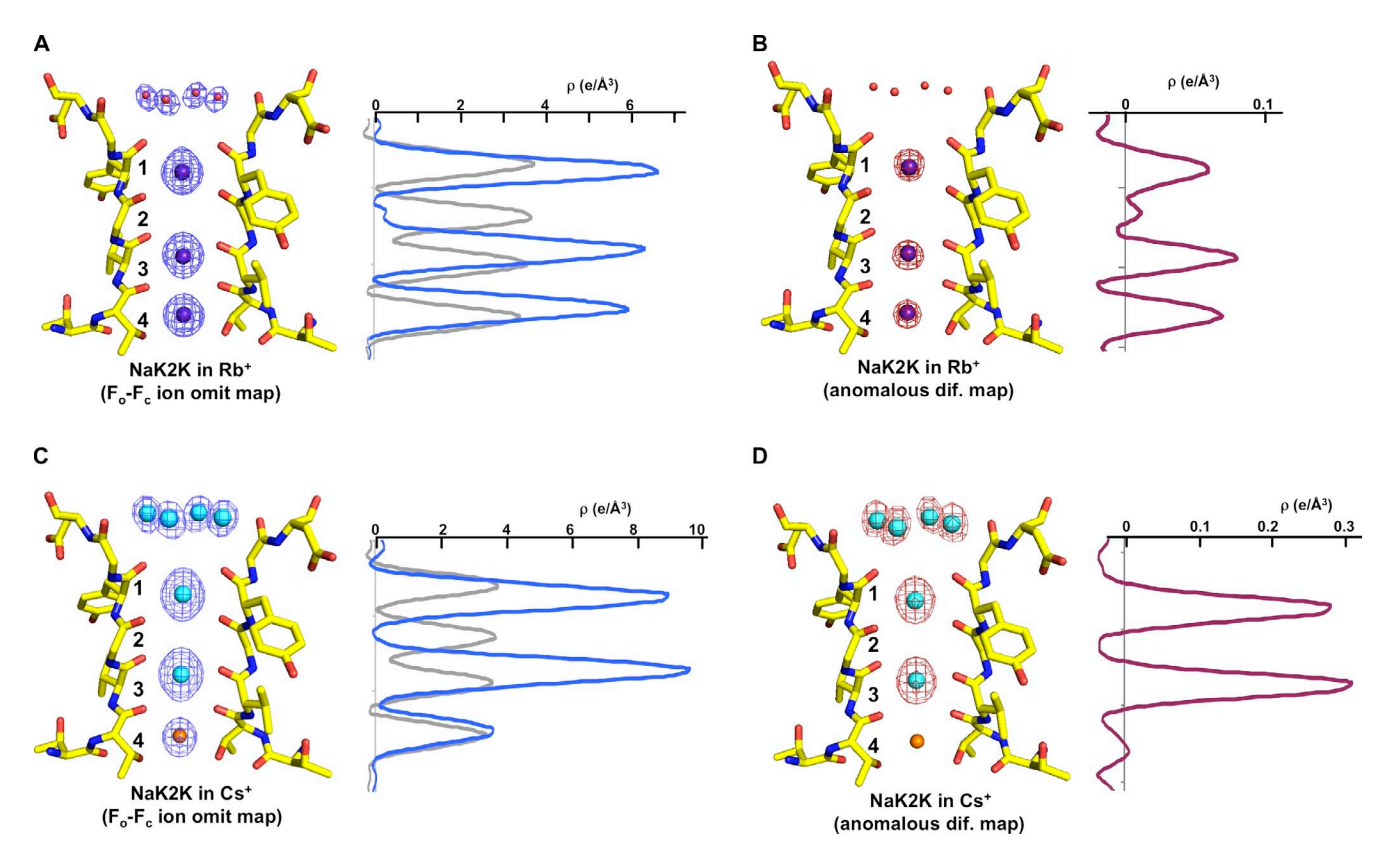


Figure 2. Rb<sup>+</sup> and Cs<sup>+</sup> binding in NaK2K. (A)  $F_o$ – $F_c$  ion omit map (6σ, blue mesh) of the NaK2K–Rb<sup>+</sup> complex and the one-dimensional electron density profile (from a 1.85-Å ion omit map) along the central axis of the filter. The electron density distribution of K<sup>+</sup> ions in the NaK2K–K<sup>+</sup> complex is also plotted (in gray) for comparison (and for all other one-dimensional profiles). The Rb<sup>+</sup> ions are modeled as purple spheres. (B) Anomalous difference Fourier map (7σ, red mesh) of the NaK2K–Rb<sup>+</sup> complex and the one-dimensional anomalous scattering profile at the selectivity filter region. (C)  $F_o$ – $F_c$  ion omit map (6σ) of the NaK2K–Cs<sup>+</sup> complex and the one-dimensional electron density profile along the filter. The Cs<sup>+</sup> ions are modeled as cyan spheres. The density at site 4 is modeled as a Na<sup>+</sup> ion (orange sphere). (D) Anomalous difference Fourier map (7σ) of the NaK2K–Cs<sup>+</sup> complex and the one-dimensional anomalous scattering profile at the selectivity filter region.

with a digitizer (Digidata 1322A; Axon Instruments). Currents were low-pass filtered at 1 kHz and sampled at 20 kHz. Except the Cs $^+$  current measurement, only patches containing a single channel were used for further experiments. Upon the observation of single-channel activity, the bath solution with 150 mM KCl was replaced by another salt as indicated in each experiment. All chemicals used for solution preparation were purchased from Sigma-Aldrich.

In the study of intracellular  $Ba^{2+}$  blocking, the free  $Ba^{2+}$  concentration was controlled by mixing 5 mM EGTA with an appropriate amount of  $BaCl_2$  calculated using the software MAXCHELATOR. Owing to the two possible orientations of reconstituted NaK2K in the liposomes,  $30~\mu M$  tetrapentyl ammonium, an intracellular pore blocker, was added in the bath solution to ensure that the channel in the recording had its intracellular side facing the bath solution for internal  $Ba^{2+}$  blocking assay and its extracellular side facing the bath solution for external  $Ba^{2+}$  blocking assay. Tetrapentyl ammonium was then removed through bath solution exchange before  $Ba^{2+}$  block measurements.

## RESULTS

Rubidium and cesium binding in the filter of NaK2K Because larger group I monovalent cations such as Rb<sup>+</sup> and Cs<sup>+</sup> are known to be permeable ions for K<sup>+</sup>-selective channels, their binding profiles in NaK2K were analyzed. The NaK2K channel was first crystallized in the presence of KCl as previously described (Derebe et al., 2011a). Crystals were then soaked into stabilization solutions in which KCl was replaced by 100 mM RbCl or CsCl, and their structures were determined to 1.58 Å and 1.7 Å, respectively (Protein Data Bank accession nos. 4PDM and 4PDL; Table 1; see Materials and methods). In both cases, the filter structures are almost identical to that of the NaK2K–K complex, with a main chain root mean square deviation (RMSD) of <0.2 Å.

The binding profile of Rb<sup>+</sup> in the NaK2K filter is similar to that of KcsA (Zhou and MacKinnon, 2003). The F<sub>o</sub>–F<sub>c</sub> ion omit map of the NaK2K–Rb<sup>+</sup> complex reveals three discrete density peaks with similar intensity at sites 1, 3, and 4, indicating equivalent Rb<sup>+</sup> binding at these three sites (Fig. 2 A). This equivalent Rb<sup>+</sup> occupancy can be further confirmed by the equivalent Rb<sup>+</sup> anomalous scattering as shown in the anomalous difference map (Fig. 2 B). To estimate the relative occupancy of Rb<sup>+</sup>, we compared the one-dimensional electron density profiles along the central axis of the filter between

TABLE 2
Filter ion occupancy

| Site/ion | $\mathrm{Rb}^{\scriptscriptstyle +}$ | Cs <sup>+</sup> | Ba <sup>2+</sup> in K <sup>+</sup> | Ba <sup>2+</sup> in Na <sup>+</sup> |
|----------|--------------------------------------|-----------------|------------------------------------|-------------------------------------|
| S0       | NA                                   | NA              | NA                                 | $0.44^{a}$                          |
| S1       | 0.69                                 | 0.68            | 0.95 (as K <sup>+</sup> ion)       | 0.24                                |
| S2       | NA                                   | NA              | NA                                 | NA                                  |
| S3       | 0.68                                 | 0.75            | 0.74 (as Ba <sup>2+</sup> ion)     | 1.00                                |
| S4       | 0.58                                 | NA              | NA                                 | NA                                  |

NA, not applicable.

the Rb<sup>+</sup> and K<sup>+</sup> complexes (see Materials and methods; Fig. 2 A and Table 2). The occupancy calculation was performed under the assumptions that the filter of the K<sup>+</sup> complex is occupied by two water molecules and two K<sup>+</sup> ions on average and that the area under the four peaks of its one-dimensional electron density profile reflects the total number of electrons in the filter (56 e-for 2 K<sup>+</sup> and 2 H<sub>2</sub>O; Zhou and MacKinnon, 2003). Accordingly, upon comparison of their one-dimensional electron density profiles, we estimated the number of electrons each Rb<sup>+</sup> peak represents and calculated the Rb<sup>+</sup> occupancy at sites 1, 3, and 4 to be 0.69, 0.68, and 0.58, respectively.

Distinct from KcsA, Cs<sup>+</sup> ions predominantly bind at sites 1 and 3 in NaK2K (Fig. 2, C and D). Although the F<sub>o</sub>-F<sub>c</sub> ion omit map of the NaK2K-Cs<sup>+</sup> complex shows three electron density peaks within the filter, the density at site 4 is clearly not coming from Cs<sup>+</sup>, as no anomalous scattering is observed at this site in the anomalous difference map. The site 4 density is likely from a mixture of water and Na<sup>+</sup> ion from the stabilization solution, which contains 100 mM Mes-NaOH buffered at pH 6. The Cs<sup>+</sup> density at sites 1 and 3 has similar intensity in both the Fo-Fc ion omit map and anomalous difference map, and the Cs<sup>+</sup> occupancy was estimated to be 0.68 and 0.75, respectively, based on the one-dimensional electron density profile. Interestingly, the fourfold symmetry-related density peaks at the external entrance is unexpectedly strong and is partially contributed by Cs<sup>+</sup>, which is indicated by the anomalous scattering signals. The equivalent density in most K<sup>+</sup> channel structures was generally weak and assigned as four water molecules for site 0 hydration shell. In light of the fourfold symmetry, the close proximity of these peaks, and the weaker anomalous scattering than the filter Cs<sup>+</sup>, we believe that each peak represents a mixture of Cs<sup>+</sup> and water molecules, with Cs<sup>+</sup> having a quarter of the occupancy. Neither Rb<sup>+</sup> nor K<sup>+</sup> seems to bind at the equivalent external site, as no obvious anomalous signal is observed in Rb<sup>+</sup>soaked crystals; and the electron density at the equivalent position is much weaker in the Rb<sup>+</sup> or K<sup>+</sup> complex and is likely from a water molecule only. It is unclear whether this off-center external Cs<sup>+</sup> binding is NaK2K specific or not.

### Rb<sup>+</sup> and Cs<sup>+</sup> permeation in NaK2K

To correlate the structurally defined ion-binding profile of Rb<sup>+</sup> and Cs<sup>+</sup> in the NaK2K filter with their permeation properties, we performed single-channel recording of NaK2K reconstituted into liposomes in the presence of Rb<sup>+</sup> or Cs<sup>+</sup> (Fig. 3). As equal distribution of two K<sup>+</sup> ions between 1,3 and 2,4 configurations appears to be essential for efficient ion permeation in K<sup>+</sup> channels (Morais-Cabral et al., 2001), the imbalanced binding of Rb<sup>+</sup> and Cs<sup>+</sup> would imply a lower permeation rate. Indeed, the single-channel conductance of NaK2K in 150 mM of symmetrical RbCl is  $\sim$ 20 pS (Fig. 3 A), much lower than that of 120 pS in KCl (Derebe et al., 2011a). With respect to selectivity, NaK2K is also slightly more selective for K<sup>+</sup> with a permeability ratio ( $P_{\rm K}/P_{\rm Rb}$ ) of  $\sim$ 1.5 (Fig. 3 B).

Cs<sup>+</sup> binds almost exclusively at sites 1 and 3 within the NaK2K filter, representing an extreme case of imbalanced ion distribution between 1,3 and 2,4 configurations. This implies a high energy difference between the two configurations and would suggest an extremely low efficiency of ion permeation. As expected, the Cs<sup>+</sup> current, if permeable, is too small to measure (Heginbotham and MacKinnon, 1993). With K<sup>+</sup> as the permeating ion, Cs<sup>+</sup> can reduce the K<sup>+</sup> current and serve as a permeating blocker similar to Ba<sup>2+</sup>, as discussed in the section below (Fig. 3 C).

External K<sup>+</sup>-dependent barium block of the NaK2K channel Ba<sup>2+</sup>, which has an identical crystal radius as K<sup>+</sup>, is known to bind K<sup>+</sup> channel filters and block the K<sup>+</sup> current. It has been shown that the kinetics of internal Ba<sup>2+</sup> blocking (mean blocking dwell time) depends on the presence of external K<sup>+</sup> (Neyton and Miller, 1988a,b; Piasta et al., 2011). To test if this also occurs in NaK2K, we performed a similar blocking assay on NaK2K using single-channel recording. In this assay, the extracellular solution (in pipette) contained 150 mM NaCl with or without K<sup>+</sup>, and the intracellular solution (bath) contained 150 mM KCl with and without BaCl<sub>2</sub>. Shown in Fig. 4 A are sample traces of outward NaK2K currents without Ba2+ (control in bi-ionic condition), with 10 μM internal Ba<sup>2+</sup> but no external K+, and with 10 µM internal Ba2+ and 5 mM external K<sup>+</sup>. In the absence of Ba<sup>2+</sup> (Fig. 4 A, top trace), NaK2K exhibits two closing states, as demonstrated by

<sup>&</sup>lt;sup>a</sup>H<sub>2</sub>O was not taken into account in the occupancy calculation for site 0 Ba<sup>2+</sup>, as water has never been observed at this site.

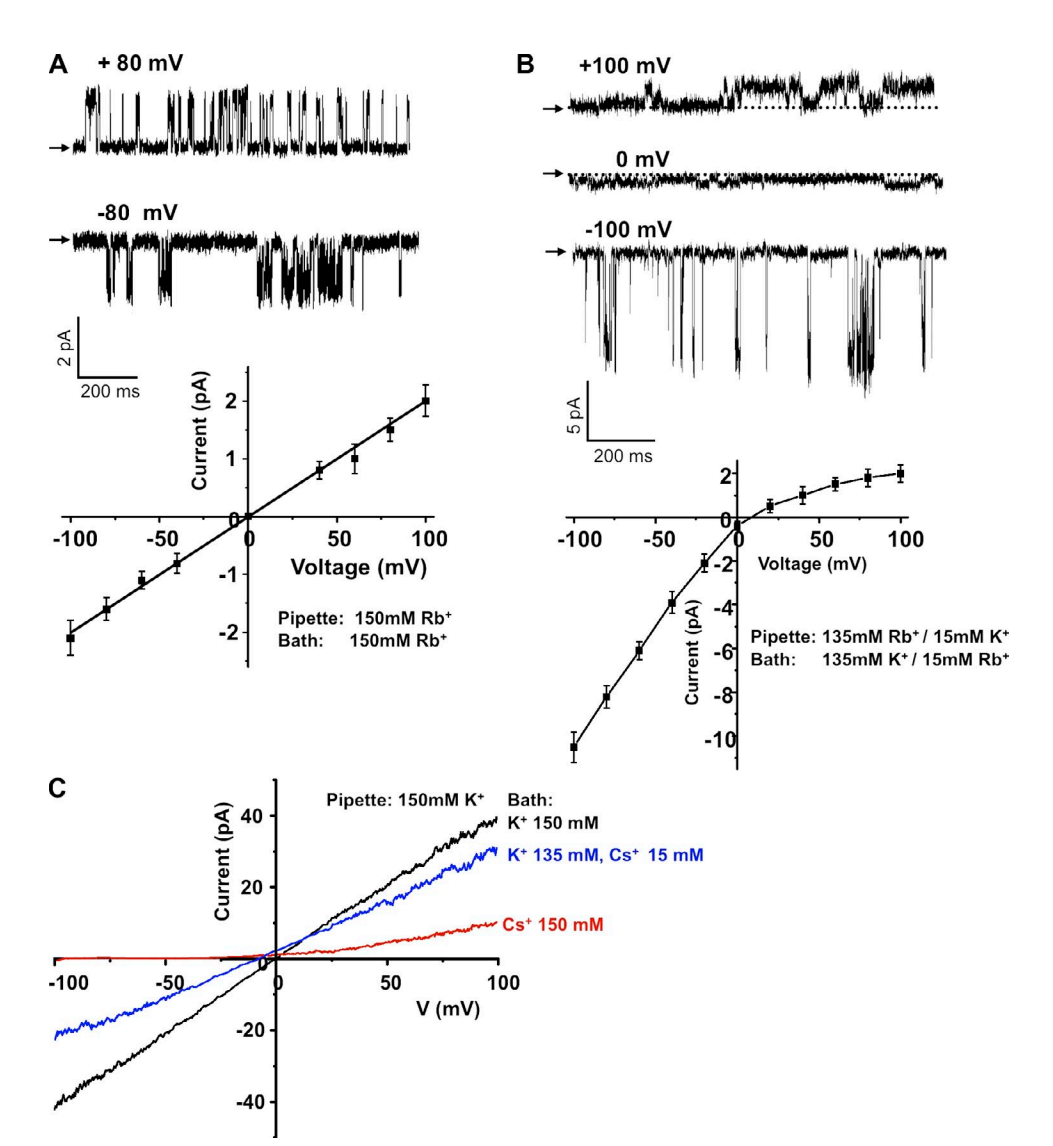


Figure 3. Rb<sup>+</sup> and Cs<sup>+</sup> permeation in NaK2K. (A) Singlechannel traces of NaK2K at ±80 mV with a symmetrical 150 mM RbCl and its I-V curve (n = 5measurements). Currents were recorded using giant liposome patch clamping. The same method was used in all other recordings. The arrows indicate the baseline. (B) Single-channel traces of NaK2K with 150 mM of a mixture of Rb+ and K+ and its I-V curve (n = 5 measurements). The channel is slightly selective for K+ with a reversal potential of  $\sim$ 10 mV. (C) The I-V curves of NaK2K in the presence and absence of Cs+. The pipette solution contains 150 mM KCl. The bath solution contains 150 mM KCl (black trace), 135 mM KCl and 15 mM CsCl (blue trace), or 150 mM CsCl (red trace). For a better assessment of reversal potential, each I-V curve was obtained from the mean of 20 current traces recorded using a patch containing multiple channels with voltage ramps from -100 to 100 mV over a 400-ms duration. Error bars represent SEM.

the nonconducting dwell time histogram: brief closings with a time constant of  $\sim 0.7$  ms ( $\tau 1$ ) and longer closings with a time constant of  $\sim 5$  ms ( $\tau 2$ ). The rapid closings are an intrinsic property of the pore and were also observed in other K+ channels with a submillisecond time constant (Li et al., 2007; Piasta et al., 2011). These spontaneous closings are likely a result of the fast gating at the filter region. The longer closings can be attributed to gating at the intracellular bundle crossing. The addition of 10 µM Ba<sup>2+</sup> at the intracellular side (Fig. 4 A, middle trace) does not change the kinetics of brief closings. However, it increases the time constant for the longer closings ( $\tau$ 2) to  $\sim$ 18 ms. This increase of closing time can be attributed to Ba<sup>2+</sup> block, which lasts longer than the kinetics of the intracellular gating. When 5 mM K<sup>+</sup> is included in the extracellular solution (5 mM KCl/145 mM NaCl), a third extremely long closing state with a time constant in the order of seconds ( $\tau$ 3,  $\sim$ 3,200 ms in this measurement) is observed. The two Ba<sup>2+</sup>-induced closing states ( $\tau$ 2 and  $\tau$ 3; Fig. 4 A, bottom trace) in the presence

of external  $K^+$  are reminiscent of the two  $Ba^{2+}$  block states with fast and slow time constants (termed  $\tau f$  and  $\tau s$ ) observed in KcsA (Piasta et al., 2011). Similar to KcsA, the time constant of fast  $Ba^{2+}$  block ( $\tau 2$ ) in NaK2K appears to be independent of external  $K^+$ , as it remains almost unchanged in the presence or absence of external  $K^+$ . The slow  $Ba^{2+}$  block ( $\tau 3$ ), however, depends on external  $K^+$ . It represents an external  $K^+$ -induced  $Ba^{2+}$  lock-in state in which external  $K^+$  binding prevents the  $Ba^{2+}$  ion in the filter from escaping to the extracellular side and prolongs  $Ba^{2+}$  block to a timescale of seconds.

We also measured the effect of external Ba<sup>2+</sup> block in NaK2K (Fig. 4 B). In this assay, the channel in the patch has its extracellular side facing the bath solution containing 145 mM NaCl and 5 mM KCl, with or without Ba<sup>2+</sup>, and the intracellular solution (in pipette) contained 150 mM KCl. Similar to other K<sup>+</sup> channels, the Ba<sup>2+</sup> block in NaK2K is also much weaker from the external side, as shown in the sample trace of outward currents with 1 mM Ba<sup>2+</sup> (Fig. 4 B). However, the external Ba<sup>2+</sup>

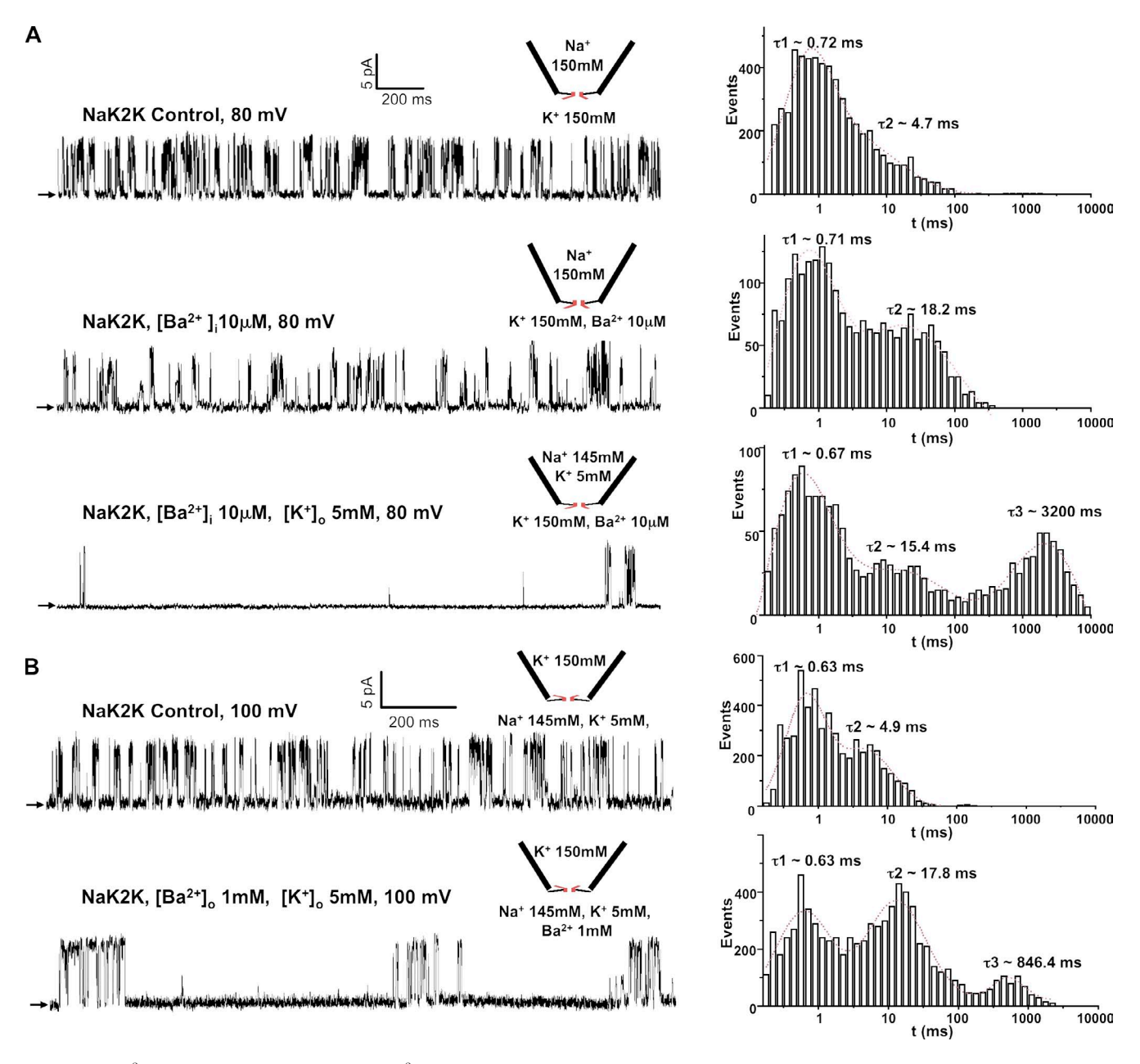


Figure 4.  $Ba^{2+}$  block in NaK2K. (A) Internal  $Ba^{2+}$  block in the presence and absence of external  $K^+$ . The nonconducting dwell time histograms with exponential fits for each recording are shown beside each trace. Only the patch that contains a channel with its intracellular side facing the bath solution was used in the recording. (B) External  $Ba^{2+}$  block in the presence of 5 mM external  $K^+$ . Only the patch that contains a channel with its extracellular side facing the bath solution was used in the recording.

still induces two block states with fast and slow time constants in the presence of external  $K^+$ , as seen in KcsA.

# Barium binding in the NaK2K filter in the presence of potassium

To examine the structural basis of the K<sup>+</sup>-dependent Ba<sup>2+</sup> block in the NaK2K channel, we soaked NaK2K crystals in a stabilization solution containing 20 mM Ba<sup>2+</sup> in addition to 100 mM K<sup>+</sup> and determined the structure to 1.82 Å (Protein Data Bank accession no. 4PDV). Although the filter structure is virtually the same as that of the NaK2K–K<sup>+</sup> complex (RMSD of 0.1 Å), the electron density

of bound ions within the filter is unevenly distributed, with the strongest density at site 3 and much weaker density at sites 2 and 4 (Fig. 5 A). As confirmed by the anomalous difference map (Fig. 5 B), Ba<sup>2+</sup> binds almost exclusively at site 3, a finding that is very different from Ba<sup>2+</sup> binding in KcsA, which occurs mainly at site 4 with weaker binding at site 2 when K<sup>+</sup> is absent (Jiang and MacKinnon, 2000; Lockless et al., 2007). Analysis of site 3 intensity in the one-dimensional electron density profile yielded a Ba<sup>2+</sup> occupancy of 0.74 (Fig. 5 A and Table 2). The presence of site 3 Ba<sup>2+</sup> excludes the K<sup>+</sup> binding at neighboring sites, resulting in much weaker density at sites 2 and 4.

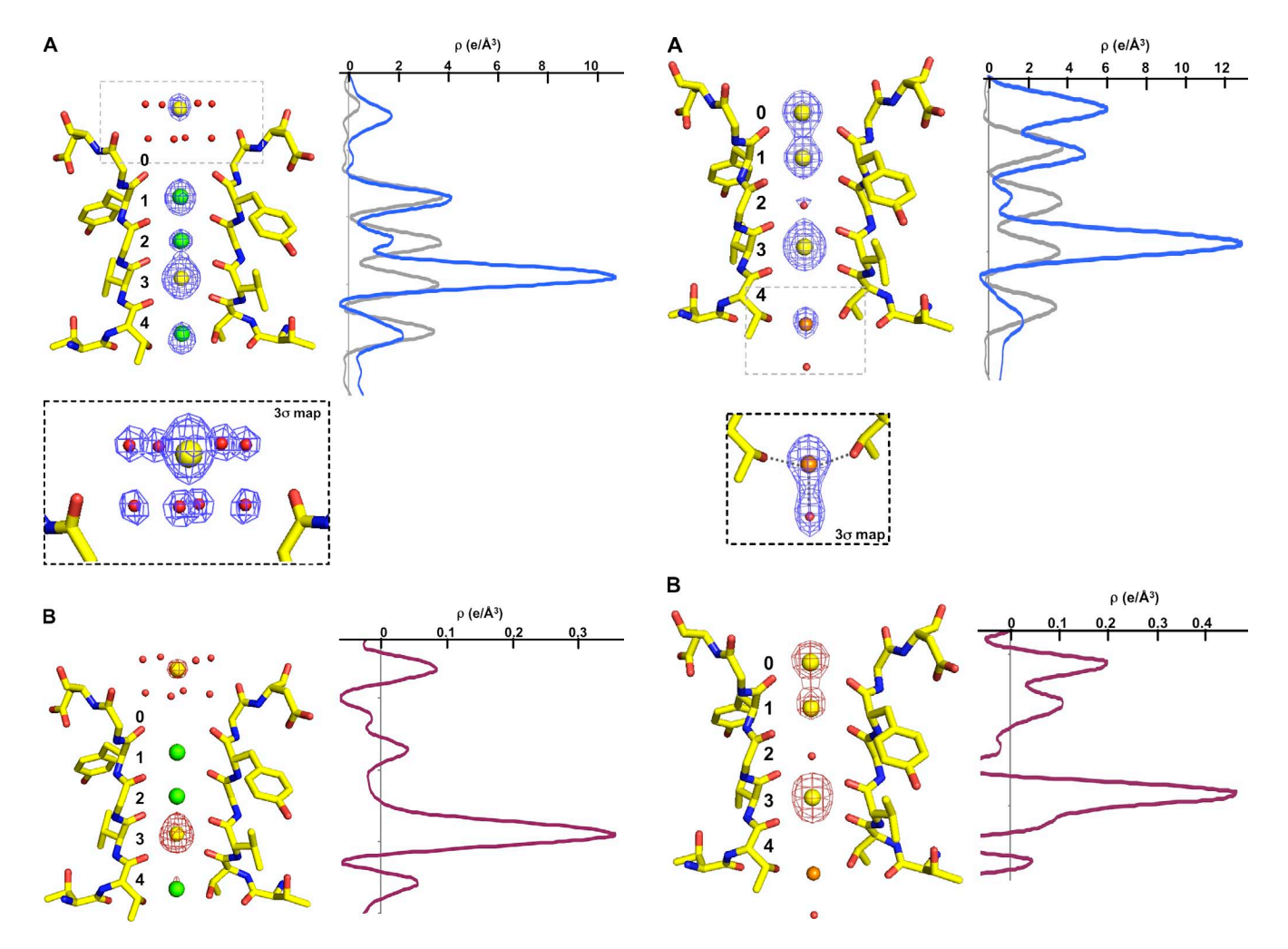


**Figure 5.** Ba<sup>2+</sup> binding in the NaK2K filter in the presence of K<sup>+</sup>. (A)  $F_o$ – $F_c$  ion omit map (6 $\sigma$ ) of the NaK2K–Ba<sup>2+</sup> complex and the one-dimensional electron density profile along the filter. The Ba<sup>2+</sup> ions are modeled as yellow spheres. The density at sites 1, 2, and 4 is modeled as K<sup>+</sup> ions (green spheres) for simplicity. The inset (boxed) is a magnified view of the external Ba<sup>2+</sup> with the  $F_o$ – $F_c$  ion omit map contoured at 3 $\sigma$  to show the density of water molecules. (B) Anomalous difference Fourier map (7 $\sigma$ ) of the NaK2K–Ba<sup>2+</sup> complex and the one-dimensional anomalous scattering profile at the selectivity filter region.

Interestingly, even with  $Ba^{2+}$  occupying site 3,  $K^+$  remains bound at site 1, as indicated by the strong electron density without obvious anomalous signal, eliminating the possibility of this density coming from  $Ba^{2+}$ . The exclusion of  $K^+$  at sites 2 and 4 upon  $Ba^{2+}$  binding actually enhances the occupancy of site 1  $K^+$  to  $\sim$ 0.95 as estimated based on the peak height in the one-dimensional electron density profile. The high occupancy of site 1  $K^+$  (close to unity) and site 3  $Ba^{2+}$  indicates that their binding at these two sites can take place simultaneously. This co-residence of  $Ba^{2+}$  at site 3 and  $K^+$  at site 1 is a snapshot of the lock-in state, which explains how  $K^+$  prevents  $Ba^{2+}$  from exiting to the extracellular side and prolongs  $Ba^{2+}$  blockage observed in our electrophysiology data. Two

**Figure 6.** Ba<sup>2+</sup> binding in the NaK2K filter in the absence of K<sup>+</sup>. (A)  $F_o$ – $F_c$  ion omit map (6σ) of the NaK2K–Ba<sup>2+</sup> complex in NaCl and the one-dimensional electron density profile along the filter. The Ba<sup>2+</sup> ions are modeled as yellow spheres. Site 2 density is modeled as water (red spheres), and site 4 density is modeled as a Na<sup>+</sup> ion (orange spheres). The inset (boxed) is a magnified view of site 4 Na<sup>+</sup> with the  $F_o$ – $F_c$  ion omit map contoured at 3σ to show the density of the cavity water molecule. (B) Anomalous difference Fourier map (7σ) of the NaK2K–Ba<sup>2+</sup> complex in NaCl and the one-dimensional anomalous scattering profile at the selectivity filter region.

observations indicate that Ba<sup>2+</sup> and Na<sup>+</sup> are also partially occupying site 4 in the crystal in addition to K<sup>+</sup>, resulting in a stronger site 4 density than that of site 2. One observation is that the site 4 ion has some weak anomalous scattering, indicating the presence of Ba<sup>2+</sup> at low occupancy. The other observation is that the site 4 density is diffusive and extended toward the bottom of site 4 where Na<sup>+</sup> typically binds (Alam and Jiang, 2009b), and the soaking solution does contain Na<sup>+</sup> from NaOH used for Mes buffering. In the structure of the NaK2K–Ba<sup>2+</sup> complex in NaCl (discussed in the next section), we did demonstrate that Na<sup>+</sup> can co-reside at the bottom of site 4 with Ba<sup>2+</sup> occupying site 3.

An additional anomalous density peak, although weak, was observed on the extracellular face of the channel just above site 0, indicating a second weak Ba<sup>2+</sup> site. The presence of external Ba<sup>2+</sup> can also be confirmed by the strong electron density that was not observed in the NaK2K–K<sup>+</sup> complex. Unlike the site 0 Ba<sup>2+</sup> seen in the NaK2K–Ba<sup>2+</sup> complex in NaCl (discussed in the next section) or the asymmetrical external Cs<sup>+</sup>, this bound Ba<sup>2+</sup> is further outside on the central axis and fully hydrated (Fig. 5 A, inset). Similar weak binding of a fully hydrated divalent cation at the external entrance has also been observed in other NaK mutants, such as a hydrated Ca<sup>2+</sup> in the NaK2CNG mutant (Derebe et al., 2011b).

# Barium binding in the NaK2K filter in the absence of potassium

To reveal the structural basis of fast Ba<sup>2+</sup> blockage in the absence of external K<sup>+</sup>, we performed a Ba<sup>2+</sup> soaking experiment in the presence of 100 mM NaCl in stabilization solution instead of KCl and determined the structure of the Ba<sup>2+</sup>/Na<sup>+</sup>-soaked NaK2K crystal to 1.85 Å (Protein Data Bank accession no. 4PDR). In the absence of K<sup>+</sup>, Ba<sup>2+</sup> binds at three positions, as demonstrated in the anomalous difference map (Fig. 6). Even though site 3 is still the major Ba<sup>2+</sup> site with full occupancy ( $\sim$ 1.0), Ba<sup>2+</sup> also binds at site 1 and site 0. Because of the close proximity of these two sites, Ba<sup>2+</sup> is unlikely to simultaneously occupy both of them. As indicated by the stronger anomalous signal, site  $0 \text{ Ba}^{2+}$  has a higher occupancy ( $\sim 0.44$ ) than that of site 1 ( $\sim$ 0.24). Despite multiple binding sites, the likelihood of having two double charged Ba<sup>2+</sup> ions within the NaK2K filter is low because of the strong electrostatic repulsion. Thus, the low probability of Ba<sup>2+</sup> binding at site 1 could be the result of high Ba<sup>2+</sup> occupancy at site 3. Nevertheless, without K<sup>+</sup> competition, Ba<sup>2+</sup> binding at site 3 as well as site 1 or 0 reveals the steps along the path of Ba<sup>2+</sup> release to the extracellular side. Although fully occupied site 3 Ba<sup>2+</sup> almost completely excludes the binding of any other ion at site 2, Na<sup>+</sup> can still reside at the bottom edge of site 4 with the coordination of Thr63 hydroxyl groups and a water molecule in the cavity as commonly seen in multiple NaK mutant structures (Fig. 6 A, inset). As sites 0 and 1 become the main secondary sites for Ba<sup>2+</sup> in the absence of K<sup>+</sup> competition, Ba<sup>2+</sup> binding is no longer observed at the external entrance above site 0.

#### DISCUSSION

By using high resolution structures along with anomalous signals, we can accurately define how various permeating and blocking cations bind in  $K^+$ -selective NaK2K channel. Combined with single-channel electrophysiology, this approach provides structural insights into ion permeation and blocking in the  $K^+$  channel. Despite the seemingly identical filter structure to canonical  $K^+$  channels,

the ion-binding profile of NaK2K shows some distinct features. Although Rb<sup>+</sup> binding in NaK2K is similar to other K<sup>+</sup> channels, Cs<sup>+</sup> in NaK2K binds mainly at sites 1 and 3 and serves as a permeating blocker. With respect to selectivity, NaK2K is slightly more selective for K<sup>+</sup> than Rb<sup>+</sup> and Cs<sup>+</sup> based on the reversal potential in bi-ionic conditions with the sequence of K<sup>+</sup> > Rb<sup>+</sup> > Cs<sup>+</sup> > Na<sup>+</sup>, which is distinct from some other K<sup>+</sup> channels (Heginbotham and MacKinnon, 1993; Hille, 2001; LeMasurier et al., 2001).

The most notable difference is the Ba<sup>2+</sup>-blocking site. In KcsA, site 4 is the primary site for Ba<sup>2+</sup>, with site 2 being the secondary site in the absence of K<sup>+</sup>. In NaK2K, Ba<sup>2+</sup> blocks primarily at site 3 with K<sup>+</sup>, if present, residing at site 1. The presence of both Ba2+ and K+ in the filter represents the so-called lock-in state of Ba<sup>2+</sup> block, where extracellular K<sup>+</sup> binding at site 1 traps the Ba<sup>2+</sup> at site 3 and prolongs the duration of Ba2+ block. The removal of external K<sup>+</sup> would allow Ba<sup>2+</sup> exit to the external side via binding at sites 1 and 0. It is also worth noting the difference in Ba<sup>2+</sup> binding between NaK2K and MthK (see Guo et al. in this issue). In MthK, Ba<sup>2+</sup> binds primarily at site 2, with secondary binding at sites 3 and 4 in the absence of K<sup>+</sup> (in a Na<sup>+</sup>-only condition). The presence of high K<sup>+</sup> can outcompete Ba<sup>2+</sup> in the filter, resulting in low occupancy Ba<sup>2+</sup> binding mainly at site 4.

Despite the difference in Ba<sup>2+</sup> binding between NaK2K and KcsA (or MthK), the principle of K<sup>+</sup>-dependent Ba<sup>2+</sup> lock-in is likely the same (Fig. 7). In the absence of external K<sup>+</sup>, the outward electrochemical driving force can quickly dislocate Ba<sup>2+</sup> from its primary blocking site (site 3 or 4) and push the ion through the filter via its secondary site (site 1 or 2). As site 1 has been shown, both structurally and functionally, to be the common K<sup>+</sup>-selective site in multiple channels (Neyton and Miller, 1988a; Spassova and Lu, 1999; Ye et al., 2010; Piasta et al., 2011; Sauer et al., 2013), the presence of external K<sup>+</sup> results in K<sup>+</sup> occupation at site 1, which prevents Ba<sup>2+</sup> from accessing its secondary site and thereby blocks its passage to the external side. In NaK2K, the external K<sup>+</sup> and the permeating Ba<sup>2+</sup> are both competing for site 1, whereas in KcsA, the K<sup>+</sup> occupation at site 1 prevents Ba<sup>2+</sup> from accessing the adjacent site (site 2) as a result of the electrostatic repulsion. With K<sup>+</sup> occupying site 1, the unblock of the filter Ba<sup>2+</sup> can occur via two pathways: either by exiting to the inside, which would be against the electrochemical gradient under most experimental conditions, or by outcompeting with site 1 K+, which depends on the K<sup>+</sup> affinity and external concentration. Either process will lead to a prolonged Ba<sup>2+</sup> block. The high K<sup>+</sup> selectivity of site 1 may also explain the weak Ba<sup>2+</sup>-blocking effect from the external side, as K+ occupation at site 1 prevents external Ba2+ from accessing its primary binding site (Fig. 4).

The observed Ba<sup>2+</sup>/K<sup>+</sup> binding profile in NaK2K is surprisingly similar to what was deduced from the Ba<sup>2+</sup> block study in BK channels by Neyton and Miller (1988a),

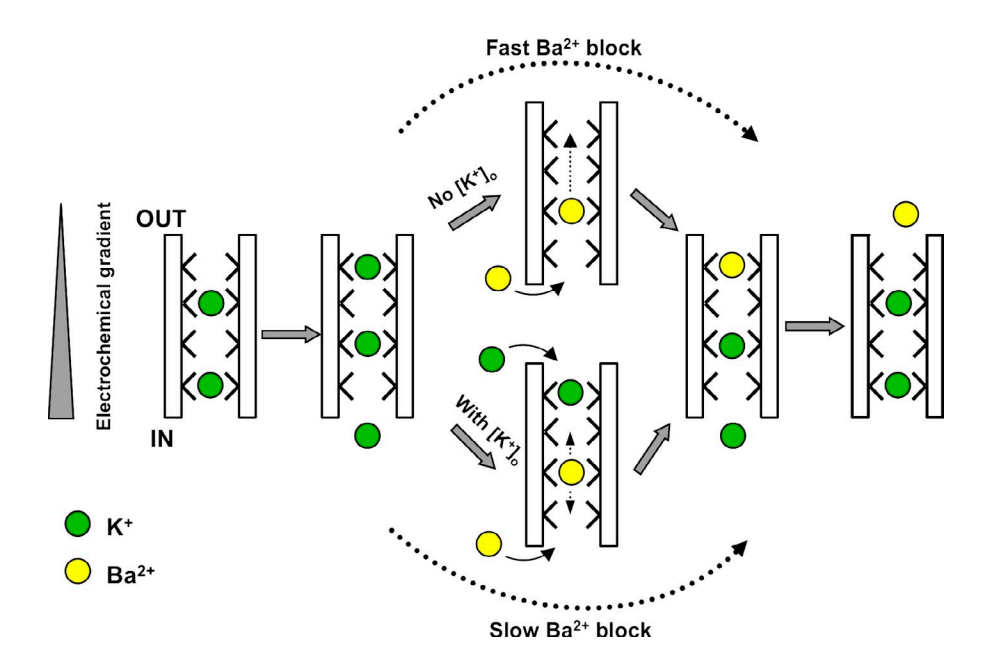


**Figure 7.** Cartoon representation of the fast (no external  $K^+$ ) and slow (with external  $K^+$ ) Ba<sup>2+</sup> blocks from the intracellular side with an outward electrochemical driving force.

which admirably was performed long before any K<sup>+</sup> channel structure was available. As recapitulated in Fig. 8, two K<sup>+</sup>-selective sites external to Ba<sup>2+</sup>, the lock-in and enhancement sites in BK, were proposed in their study. The highly K<sup>+</sup>-selective lock-in site is equivalent to site 1 and has high K<sup>+</sup> affinity even in the presence of Ba<sup>2+</sup>, consistent with the co-residence of site 1 K<sup>+</sup> and site 3 Ba<sup>2+</sup> observed in the NaK2K filter. The enhancement site, equivalent to site 2, is adjacent to Ba<sup>2+</sup> and can only start to be occupied by K<sup>+</sup> at high concentration, consistent with low K<sup>+</sup> occupancy in our structure. Their study also revealed another low selective lock-in site internal to Ba<sup>2+</sup>, which is equivalent to site 4. Indeed, our previous selectivity study of NaK2K did demonstrate that sites 1 and 2 are the two most K<sup>+</sup> preferred sites, whereas

site 4 is the least K<sup>+</sup> selective one, which can also be occupied by Na<sup>+</sup> even in the presence of Ba<sup>2+</sup> at site 3, as we show here (Sauer et al., 2013).

Given the high conservation of filter architecture in all K<sup>+</sup> channels, it remains a mystery why these seemingly identical K<sup>+</sup> channel filters exhibit quite different ion binding profiles, most notably in K<sup>+</sup> and Ba<sup>2+</sup>. As demonstrated in our previous study, when competing against Na<sup>+</sup>, K<sup>+</sup> clearly prefers sites 1 and 2 in NaK2K (Sauer et al., 2013), whereas sites 1 and 3 are preferred in MthK (Ye et al., 2010). In this study, we demonstrated that the primary and secondary binding sites for Ba<sup>2+</sup> in NaK2K are sites 3 and 1 (or 0), respectively, whereas in KcsA they are sites 4 and 2, respectively (Lockless et al., 2007). Even within the same channel filter, K<sup>+</sup> appears to prefer two

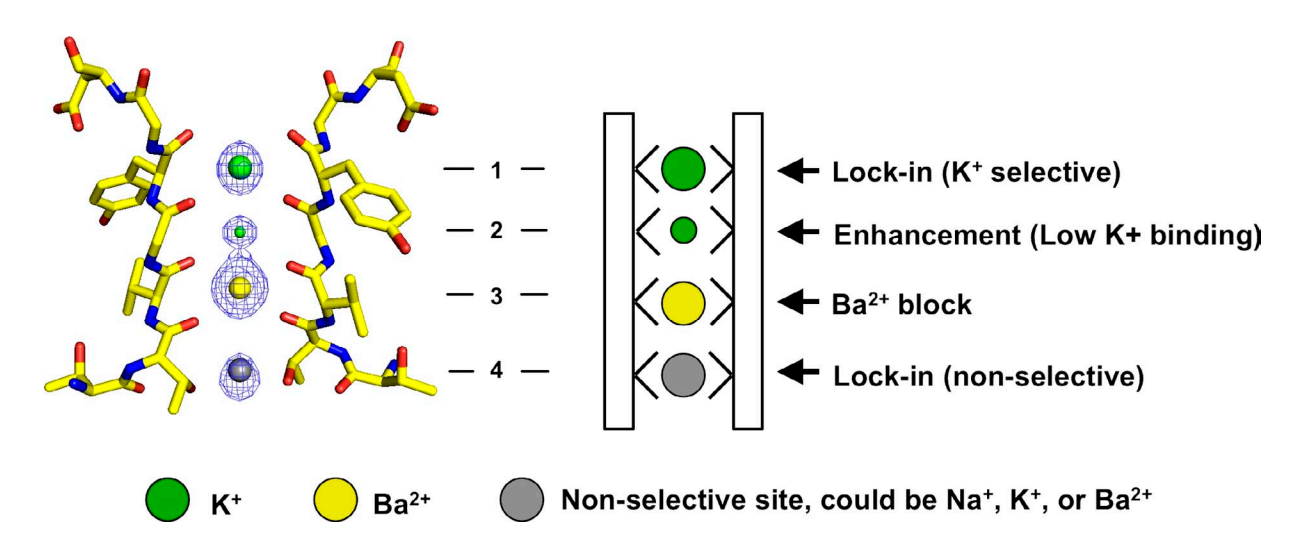


Figure 8. Comparison of the structural snapshot of the  $Ba^{2+}/K^+$  binding profile in NaK2K filter with the multi-ion binding sites deduced from the  $Ba^{2+}$  block study in BK channels. The sizes of the green spheres are scaled to represent  $K^+$  affinity (occupancy). The site 4 ion is represented by a gray sphere to indicate the nonselective nature of the site.

particular sites at low concentrations, even though all four sites within the filter have very similar structures and chemical environments. The origin of these differences remains elusive even with the available high resolution structures and warrant further investigation.

Results shown in this study are derived from work performed at the Argonne National Laboratory, Structural Biology Center (19ID), and GM/CA (23ID) at the Advanced Photon Source and from work performed at the Berkeley Center for Structural Biology at the Advanced Light Source. Argonne is operated by the University of Chicago Argonne, LLC, for the U.S. Department of Energy, Office of Biological and Environmental Research under contract DE-AC02-06CH11357. The Berkeley Center for Structural Biology is supported in part by the National Institutes of Health, National Institute of General Medical Sciences, and the Howard Hughes Medical Institute. The Advanced Light Source is supported by the Director, Office of Science, Office of Basic Energy Sciences, of the U.S. Department of Energy under contract no. DE-AC02-05CH11231.

This work was supported in part by the Howard Hughes Medical Institute and by grants from the National Institutes of Health (grant GM079179 to Y. Jiang) and the Welch Foundation (grant I-1578 to Y. Jiang).

The authors declare no competing financial interests.

Kenton J. Swartz served as editor.

Submitted: 28 February 2014 Accepted: 25 June 2014

#### REFERENCES

- Adams, P.D., P.V. Afonine, G. Bunkóczi, V.B. Chen, I.W. Davis, N. Echols, J.J. Headd, L.W. Hung, G.J. Kapral, R.W. Grosse-Kunstleve, et al. 2010. *PHENIX*: a comprehensive Python-based system for macromolecular structure solution. *Acta Crystallogr. D Biol. Crystallogr.* 66:213–221. http://dx.doi.org/10.1107/S0907444909052925
- Alam, A., and Y. Jiang. 2009a. High-resolution structure of the open NaK channel. *Nat. Struct. Mol. Biol.* 16:30–34. http://dx.doi.org/10 .1038/nsmb.1531
- Alam, A., and Y. Jiang. 2009b. Structural analysis of ion selectivity in the NaK channel. *Nat. Struct. Mol. Biol.* 16:35–41. http://dx.doi.org/10.1038/nsmb.1537
- Alam, A., and Y. Jiang. 2011. Structural studies of ion selectivity in tetrameric cation channels. *J. Gen. Physiol.* 137:397–403. http://dx.doi.org/10.1085/jgp.201010546
- Andersen, O.S. 2011. Perspectives on: Ion selectivity. *J. Gen. Physiol.* 137:393–395. http://dx.doi.org/10.1085/jgp.201110651
- Armstrong, C.M., and S.R. Taylor. 1980. Interaction of barium ions with potassium channels in squid giant axons. *Biophys. J.* 30:473–488. http://dx.doi.org/10.1016/S0006-3495(80)85108-3
- Armstrong, C.M., R.P. Swenson Jr., and S.R. Taylor. 1982. Block of squid axon K channels by internally and externally applied barium ions. J. Gen. Physiol. 80:663–682. http://dx.doi.org/10.1085/jgp.80.5.663
- Derebe, M.G., D.B. Sauer, W. Zeng, A. Alam, N. Shi, and Y. Jiang. 2011a. Tuning the ion selectivity of tetrameric cation channels by changing the number of ion binding sites. *Proc. Natl. Acad. Sci. USA*. 108:598–602. http://dx.doi.org/10.1073/pnas.1013636108
- Derebe, M.G., W. Zeng, Y. Li, A. Alam, and Y. Jiang. 2011b. Structural studies of ion permeation and Ca<sup>2+</sup> blockage of a bacterial channel mimicking the cyclic nucleotide-gated channel pore. *Proc. Natl. Acad. Sci. USA*. 108:592–597. http://dx.doi.org/10.1073/pnas.1013643108
- Dixit, P.D., and D. Asthagiri. 2011. Thermodynamics of ion selectivity in the KcsA K<sup>+</sup> channel. *J. Gen. Physiol.* 137:427–433. http://dx.doi.org/10.1085/jgp.201010533

- Doyle, D.A., J. Morais Cabral, R.A. Pfuetzner, A. Kuo, J.M. Gulbis, S.L. Cohen, B.T. Chait, and R. MacKinnon. 1998. The structure of the potassium channel: Molecular basis of K<sup>+</sup> conduction and selectivity. *Science.* 280:69–77. http://dx.doi.org/10.1126/science.280.5360.69
- Eaton, D.C., and M.S. Brodwick. 1980. Effects of barium on the potassium conductance of squid axon. *J. Gen. Physiol.* 75:727–750. http://dx.doi.org/10.1085/jgp.75.6.727
- Eisenman, G., R. Latorre, and C. Miller. 1986. Multi-ion conduction and selectivity in the high-conductance Ca++-activated K+channel from skeletal muscle. *Biophys. J.* 50:1025–1034. http://dx.doi.org/10.1016/S0006-3495(86)83546-9
- Emsley, P., and K. Cowtan. 2004. Coot: model-building tools for molecular graphics. *Acta Crystallogr. D Biol. Crystallogr.* 60:2126–2132. http://dx.doi.org/10.1107/S0907444904019158
- Guo, R., W. Zeng, H. Cui, L. Chen, and S. Ye. 2014. Ionic interactions of Ba<sup>2+</sup> blockades in the MthK K<sup>+</sup> channel. *J. Gen. Physiol.* 144:193–200.
- Harris, R.E., H.P. Larsson, and E.Y. Isacoff. 1998. A permanent ion binding site located between two gates of the *Shaker* K<sup>+</sup> channel. *Biophys. J.* 74:1808–1820. http://dx.doi.org/10.1016/S0006-3495(98)77891-9
- Heginbotham, L., and R. MacKinnon. 1993. Conduction properties of the cloned Shaker K+ channel. *Biophys. J.* 65:2089–2096. http://dx.doi.org/10.1016/S0006-3495(93)81244-X
- Heginbotham, L., Z. Lu, T. Abramson, and R. MacKinnon. 1994. Mutations in the K+ channel signature sequence. *Biophys. J.* 66:1061–1067. http://dx.doi.org/10.1016/S0006-3495(94)80887-2
- Hille, B. 2001. Ionic Channels of Excitable Membranes. Third edition. Sinauer Associates, Sunderland, MA. 814 pp.
- Jiang, Y., and R. MacKinnon. 2000. The barium site in a potassium channel by x-ray crystallography. J. Gen. Physiol. 115:269–272. http://dx.doi.org/10.1085/jgp.115.3.269
- Kleywegt, G.J., and T.A. Jones. 1996. *xdlMAPMAN* and *xdlDATA-MAN* programs for reformatting, analysis and manipulation of biomacromolecular electron-density maps and reflection data sets. *ActaCrystallogr.DBiol. Crystallogr.*52:826–828.http://dx.doi.org/10.1107/S0907444995014983
- LeMasurier, M., L. Heginbotham, and C. Miller. 2001. KcsA: It's a potassium channel. *J. Gen. Physiol.* 118:303–314. http://dx.doi.org/10.1085/jgp.118.3.303
- Li, Y., I. Berke, L. Chen, and Y. Jiang. 2007. Gating and inward rectifying properties of the MthK K<sup>+</sup> channel with and without the gating ring. *J. Gen. Physiol.* 129:109–120. http://dx.doi.org/10.1085/jgp.200609655
- Lockless, S.W., M. Zhou, and R. MacKinnon. 2007. Structural and thermodynamic properties of selective ion binding in a K<sup>+</sup> channel. *PLoS Biol.* 5:e121. http://dx.doi.org/10.1371/journal.pbio .0050121
- Miller, C. 1987. Trapping single ions inside single ion channels. *Biophys. J.* 52:123–126. http://dx.doi.org/10.1016/S0006-3495(87)83196-X
- Morais-Cabral, J.H., Y. Zhou, and R. MacKinnon. 2001. Energetic optimization of ion conduction rate by the K<sup>+</sup> selectivity filter. *Nature*. 414:37–42. http://dx.doi.org/10.1038/35102000
- Neyton, J., and C. Miller. 1988a. Discrete Ba2+ block as a probe of ion occupancy and pore structure in the high-conductance Ca2+-activatedK+channel. *J. Gen. Physiol.* 92:569–586. http://dx.doi.org/10.1085/jgp.92.5.569
- Neyton, J., and C. Miller. 1988b. Potassium blocks barium permeation through a calcium-activated potassium channel. *J. Gen. Physiol.* 92:549–567. http://dx.doi.org/10.1085/jgp.92.5.549
- Nimigean, C.M., and T.W. Allen. 2011. Origins of ion selectivity in potassium channels from the perspective of channel block. *J. Gen. Physiol.* 137:405–413. http://dx.doi.org/10.1085/jgp.201010551
- Otwinowski, Z., and W. Minor. 1997. Processing of X-ray diffraction data collected in oscillation mode. *Methods Enzymol.* 276:307–326. http://dx.doi.org/10.1016/S0076-6879(97)76066-X

- Piasta, K.N., D.L. Theobald, and C. Miller. 2011. Potassium-selective block of barium permeation through single KcsA channels. J. Gen. Physiol. 138:421–436. http://dx.doi.org/10.1085/jgp.201110684
- Roux, B., S. Bernèche, B. Egwolf, B. Lev, S.Y. Noskov, C.N. Rowley, and H. Yu. 2011. Ion selectivity in channels and transporters. *J. Gen. Physiol.* 137:415–426. http://dx.doi.org/10.1085/jgp.201010577
- Sauer, D.B., W. Zeng, S. Raghunathan, and Y. Jiang. 2011. Protein interactions central to stabilizing the K<sup>+</sup> channel selectivity filter in a four-sited configuration for selective K+ permeation. *Proc. Natl. Acad. Sci. USA*. 108:16634–16639. http://dx.doi.org/10.1073/pnas.1111688108
- Sauer, D.B., W. Zeng, J. Canty, Y. Lam, and Y. Jiang. 2013. Sodium and potassium competition in potassium-selective and non-selective channels. *Nat. Commun.* 4:2721. http://dx.doi.org/10.1038/ ncomms3721
- Spassova, M., and Z. Lu. 1999. Tuning the voltage dependence of tetraethylammonium block with permeant ions in an inward-rectifier K+channel. *J. Gen. Physiol.* 114:415–426. http://dx.doi.org/10.1085/ jgp.114.3.415
- Varma, S., D.M. Rogers, L.R. Pratt, and S.B. Rempe. 2011. Perspectives on: Ion selectivity. Design principles for K<sup>+</sup> selectivity in

- membrane transport. *J. Gen. Physiol.* 137:479–488. http://dx.doi.org/10.1085/jgp.201010579
- Vergara, C., and R. Latorre. 1983. Kinetics of Ca2+-activated K+ channels from rabbit muscle incorporated into planar bilayers. Evidence for a Ca2+ and Ba2+ blockade. *J. Gen. Physiol.* 82:543–568. http://dx.doi.org/10.1085/jgp.82.4.543
- Vergara, C., O. Alvarez, and R. Latorre. 1999. Localization of the K<sup>+</sup> lock-in and the Ba<sup>2+</sup> binding sites in a voltage-gated calcium-modulated channel. Implications for survival of K<sup>+</sup> permeability. *J. Gen. Physiol.* 114:365–376. http://dx.doi.org/10.1085/jgp.114.3.365
- Ye, S., Y. Li, and Y. Jiang. 2010. Novel insights into K<sup>+</sup> selectivity from high-resolution structures of an open K<sup>+</sup> channel pore. *Nat. Struct. Mol. Biol.* 17:1019–1023. http://dx.doi.org/10.1038/nsmb.1865
- Zhou, Y., and R. MacKinnon. 2003. The occupancy of ions in the K<sup>+</sup> selectivity filter: Charge balance and coupling of ion binding to a protein conformational change underlie high conduction rates. *J. Mol. Biol.* 333:965–975. http://dx.doi.org/10.1016/j.jmb.2003.09.022
- Zhou, Y., J.H. Morais-Cabral, A. Kaufman, and R. MacKinnon. 2001. Chemistry of ion coordination and hydration revealed by a K<sup>+</sup> channel-Fab complex at 2.0 Å resolution. *Nature.* 414:43–48. http://dx.doi.org/10.1038/35102009